

The Influence of the Madden–Julian Oscillation on Ocean Surface Heat Fluxes and Sea Surface Temperature

CHARLES JONES

Institute for Computational Earth System Science, University of California, Santa Barbara, California

DUANE E. WALISER

Institute for Terrestrial and Planetary Atmospheres, State University of New York at Stony Brook, Stony Brook, New York

CATHERINE GAUTIER

Institute for Computational Earth System Science and Department of Geography, University of California, Santa Barbara, California

(Manuscript received 20 September 1996, in final form 30 April 1997)

ABSTRACT

The Madden–Julian oscillation (MJO) involves pronounced variations in convection and large-scale circulation throughout the tropical troposphere. In addition, the MJO is also related to dynamic and thermodynamic variability near the surface and the upper ocean. This study uses observational data to characterize the changes in surface heat fluxes and sea surface temperature (SST) during the life cycle of the MJO.

Variations in convective activity are described with outgoing longwave radiation (OLR) during the period January 1985 through September 1994. International Satellite Cloud Climatology Project data (January 1985–April 1991) and European Centre for Medium-Range Weather Forecasts surface analyses (January 1985–December 1994) are used to derive surface fluxes of net shortwave radiation (SW), latent heat (E), their difference ($Q = SW - E$), and SST.

The spatial patterns of OLR, SW, E , Q , and SST anomalies reveal that the region of positive OLR anomalies that precede the occurrence of enhanced convection is associated with positive SW and negative E anomalies, which result in positive Q anomalies. The prevailing conditions in the region of positive Q anomalies favor the development of positive SST anomalies, which lead to variations of enhanced convection. In contrast the region of negative OLR anomalies is associated with negative SW and positive E anomalies. These conditions induce negative Q anomalies, which favor the formation of negative SST anomalies. The above results suggest a possible feedback between the oscillation and intraseasonal variations in SST and this may be an important mechanism for numerical simulations of the life cycle of the MJO.

1. Introduction

On intraseasonal timescales (30–60 days), the Madden–Julian oscillation (MJO) is the primary mode in the tropical atmosphere (Madden and Julian 1994). The MJO manifests itself as a slow eastward propagation of atmospheric disturbances with maximum amplitudes in the Eastern Hemisphere (Wang and Rui 1990; Hayashi and Golder 1993; Hendon and Salby 1994, hereafter HS94). Since its discovery by Madden and Julian (1971) over two decades ago, the MJO has continued to be a topic of significant interest due to the wide range of phenomena it interacts with. These include interaction with the extratropics, which may influence weather forecasts on medium and extended ranges (Chen and Alpert

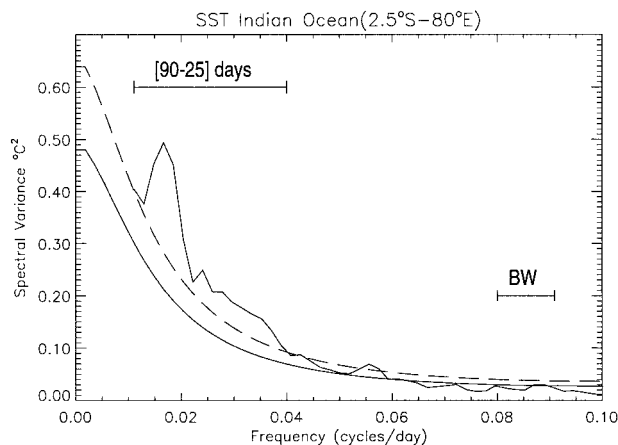


FIG. 1. Ensemble spectrum of SST over a reference site in the Indian Ocean (2.5°S, 80°E). Period: 1985–94. Smoothed solid line represents the background red-noise spectrum and dashed line is the 95% significance level. The band (25–90) days is indicated in the upper-left corner, and BW denotes the spectrum bandwidth.

Corresponding author address: Dr. Charles Jones, Earth Space Research Group, ICESS, University of California, Santa Barbara, CA 93106-3060.

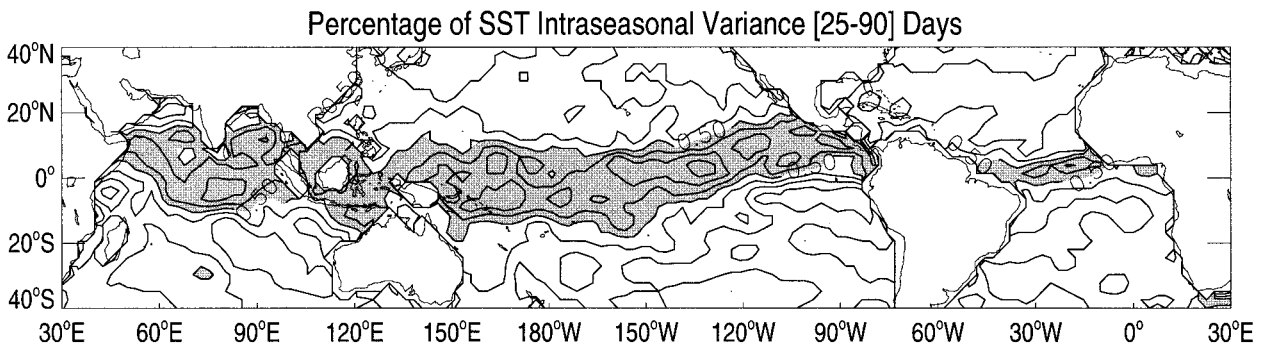


FIG. 2. Percentage of annual variance contained in the (25–90) days band (excluding the annual cycle). The field derives from the ensemble spectrum of SST (1985–94) at every grid point and is computed by dividing the variance in the band (25–90) days by the total spectral variance. Contour interval is 0.05. Shaded region denotes percentage of intraseasonal variance greater than 0.5 and exceeds the background red-noise spectrum at 95% significant level.

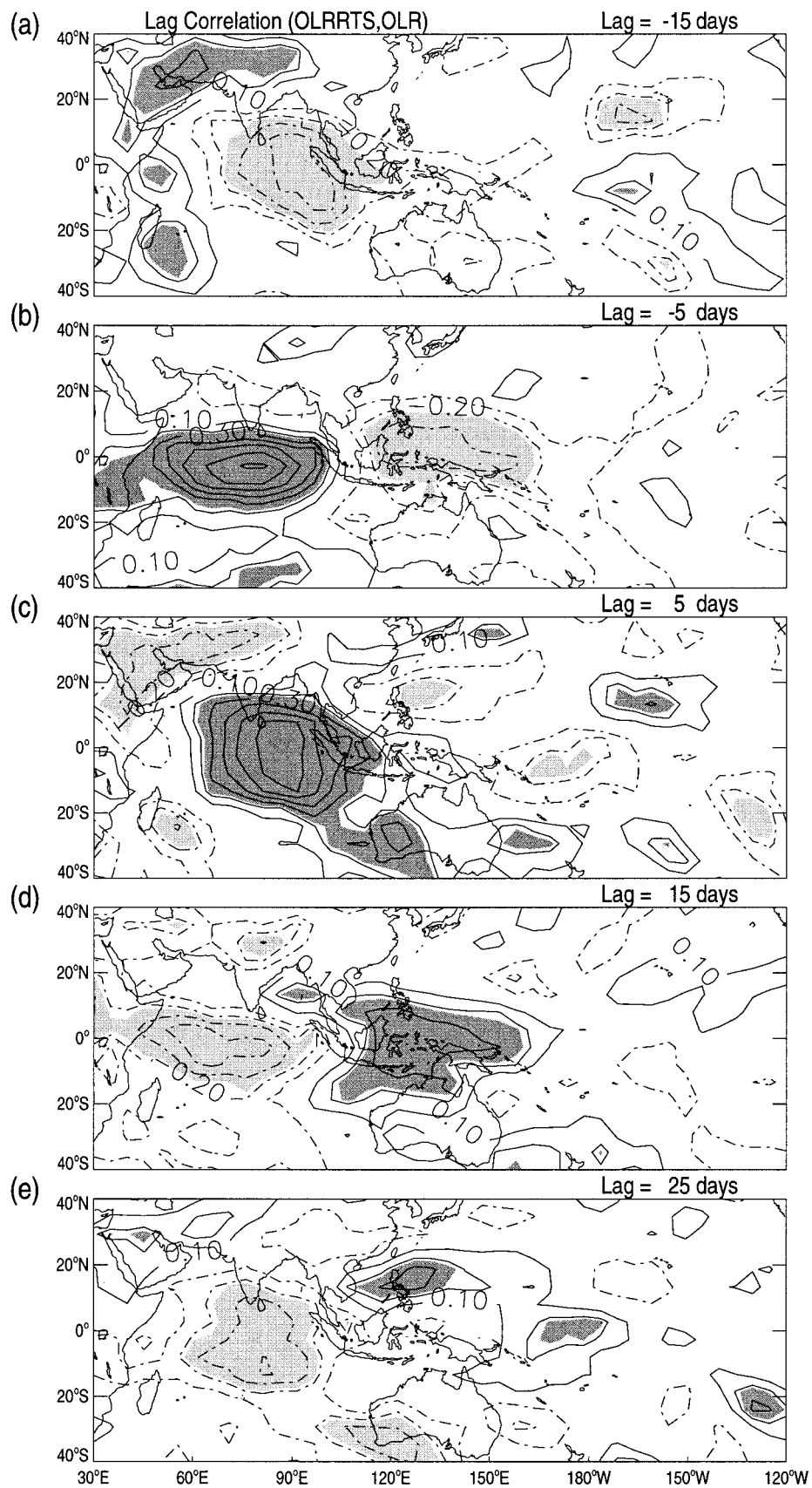
1990; Ferranti et al. 1990; Lau and Chang 1992); the Indian Monsoon system (Lau and Chan 1986a); and the tropical ocean via the strong westerly wind bursts that are associated with the occurrence of an MJO. This latter interaction has even been suggested to play an important role in the onset of El Niño events (Lau and Chan 1986b; Enfield 1987; Weickmann 1991).

Studies of near-surface parameters and upper ocean have also detected the MJO signature (Krishnamurti et al. 1988; McPhaden and Hayes 1991; Zhang and McPhaden 1995; Jones and Weare 1996; Zhang 1996). Indeed, since the MJO is characterized by timescales long enough to interact with the upper ocean, the MJO has been found to be linked to sea surface temperature (SST) variations in the Indian and Pacific Oceans (Kawamura 1988; Waliser 1996; Zhang 1996). Wang and Rui (1990), for example, pointed out that the annual cycle of SST in the Indian Ocean monsoon region can be a determining factor in the spatial and annual variations of the MJO. Furthermore, in a theoretical work, Li and Wang (1994) considered the effect of meridional gradients of SST on intraseasonal variations and showed that the northward and southward propagation of intraseasonal modes are sensitive to the spatial variability of SST. Kessler et al. (1995) were able to connect intraseasonal variations in convection to the generation of intraseasonal Kelvin waves in the eastern Pacific Ocean. Their analysis shows that westerly wind bursts following a succession of eastward propagating MJO convective anomalies excite oceanic Kelvin waves that propagate farther east across the basin. They also show, using a simplified model analysis, that nonlinear interaction between the MJO forcing and the oceanic response results in a slow eastward movement of high SST and

convection across the Pacific Ocean bearing some similarities with the onset of El Niño. Previous studies have provided some insight on the atmosphere–ocean coupling on intraseasonal timescales. However, our knowledge of how the MJO modifies SST in the Indian and Pacific Oceans (Waliser 1996), how SST variations may feedback into the oscillation, and how it may even be related to the onset of El Niño is still very incomplete.

The objective of this study is to examine the observed large-scale patterns of surface heat fluxes and SST anomalies during the life cycle of the MJO. A thorough understanding of the interaction of the MJO with the surface energy balance is important for a variety of reasons. Because the MJO involves eastward propagating modes, the oscillation has spatial patterns that are asymmetrical in the zonal direction (HS94). The zonal asymmetry of the MJO introduces complex modifications in the components of the surface energy balance. Although this topic has been sparsely addressed in previous observational studies (Kawamura 1988; Krishnamurti et al. 1988; Jones and Weare 1996; Zhang 1996), our aim is to provide an integrated view of the modifications that occur in the surface heat fluxes and SST, and to complement other studies that addressed the tropospheric life cycle of the MJO (e.g., HS94). This is done by first describing the datasets (section 2) and then examining the spatial distribution of the intraseasonal signal in SST over the global Tropics (section 3). Next, a statistical description of both time-lagged covariability and time lag composites show variations in enhanced/suppressed convective activity and anomalies in surface heat flux and SST during the life cycle of the MJO (section 4). Section 5 summarizes and discusses the results.

FIG. 3. Lag correlation patterns between OLR reference time series (OLRRTS) in the Indian Ocean (5°S–5°N; 80°–90°E) and OLR anomalies. Time lag starts at –15 days and the interval is 10 days. Solid (dashed-dotted) contours denote positive (negative) correlations starting at 0.1 (–0.1) with 0.1 interval. Heavy (light) shaded regions indicate correlations greater (less) than 0.23 (–0.23) and are significant at 95% significance level based on local t test.



2. Data

The life cycle of the MJO is characterized in this study by variations in tropical convection, specifically those that occur at the intraseasonal timescale. In this study, we use the outgoing longwave radiation (OLR) dataset, which has been frequently used as a proxy for large-scale tropical convective activity (see Waliser et al. 1993). In order to filter high-frequency variations, pentad averaging (5-day nonoverlapping means with 73 pentads yr^{-1}) is applied to the OLR, as well as all subsequently discussed fields. The OLR pentads are constructed by averaging the twice-daily observations (0000 and 1200 UTC) and have spatial resolution of $2.5^\circ \text{ lat} \times 2.5^\circ \text{ long}$. The data record extends from 1–5 January 1985 through 8–12 September 1994 (total of 708 pentads). Additional information on changes in instrumentation, equator-crossing times, and inherent biases in the OLR data can be found in Chelliah and Arkin (1992) and Waliser and Zhou (1997).

We focus our attention on two components of the surface energy balance: net shortwave radiation and latent heat flux. The net surface shortwave radiation flux (SW) is obtained from the method developed by Gautier et al. (1980), which uses input parameters derived from the International Satellite Cloud Climatology Project (ISCCP) (Rossow et al. 1988). The method to compute SW takes into account the most important radiative processes affecting the shortwave radiation transfer in the atmosphere—that is, scattering and absorption by molecules, clouds, and aerosols. It has been shown to agree well with daily surface observations under clear-sky conditions: root-mean-squared (rms) errors of 10 W m^{-2} and mean bias of 2.8 W m^{-2} (satellite minus surface observation). For partly cloudy conditions the rms and bias increase to 20 and -2.5 W m^{-2} , respectively. Under overcast conditions, the performance of the model degrades to rms of 22 W m^{-2} and bias of 13.9 W m^{-2} . A better agreement between surface observations and satellite estimates is found on monthly averages. Gautier and Landsfeld (1997) describe additional details on the latest model version and the comparison with surface observations. Pentads of SW with spatial resolution of $2.5^\circ \text{ lat} \times 2.5^\circ \text{ long}$ are used for the period 1–5 January 1985 through 26–30 April 1991 (total of 462 pentads), constrained in length by the availability of ISCCP data.

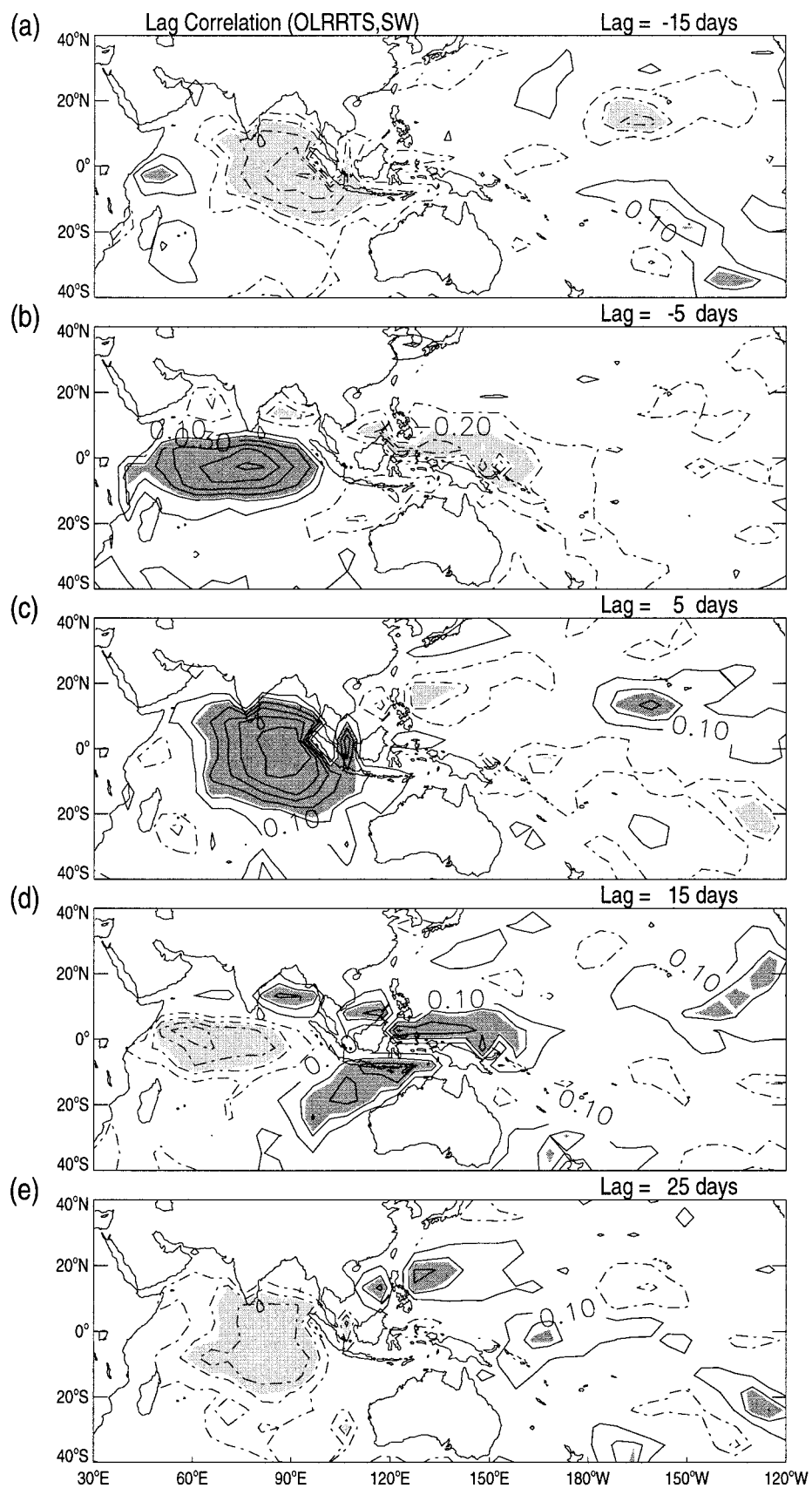
Surface latent heat flux (E) is estimated with European Centre for Medium-Range Weather Forecasts (ECMWF) surface analyses, which provide surface pressure (P_s), surface wind speeds (V_s) at 10-m height, sea surface temperature (SST), air temperature (T_a), and dewpoint temperature (T_d) at 2-m height. Daily averages of E are derived from the bulk formula and the similarity

theory model developed by Liu et al. (1979) with input parameters P_s , V_s , SST, T_a , and T_d . Pentads of E are then computed for the period 1–5 January 1985 through 26–31 December 1994 (total of 730 pentads). The estimation of E with ECMWF surface analyses has been shown to exhibit significant spectral peaks on 30–60 days and be consistent with variations in the large-scale circulation associated with the MJO (Jones and Weare 1996, hereafter JW96).

The surface heat flux is approximated by $Q = \text{SW} - E$. Since the available data for SW and E do not completely overlap in time, pentads of Q for the period 1–5 January 1985 through 26–30 April 1991 (total of 462 pentads) are used. In addition, intraseasonal variations in SST are investigated using the ECMWF SST analysis. The ECMWF SST analyses are derived from the National Centers for Environmental Prediction (NCEP) SST analyses as input data and additional modifications internal to the ECMWF data assimilation system. The NCEP SST analyses, which are based on the optimal interpolation scheme, are produced daily and weekly using in situ data (ship and buoy) and bias-corrected satellite data [for further details, see the technical report issued by ECMWF (1992) and Reynolds and Smith (1994)]. It is important to note that the SST analyses are representative of the bulk temperature, which is usually colder than the skin temperature and can lead to errors in estimating the surface heat fluxes (Fairall et al. 1996). In this study, no adjustments have been made in the ECMWF SST analyses. Pentads from 1–5 January 1985 through 26–31 January 1994 (total of 730 pentads) are used.

Some of the datasets described above (OLR, SW, E , Q) have a very small fraction (less than 5%) of the total period with missing observations, and these were linearly interpolated in time. Also, it should be pointed out that uncertainties present in all of the above fields are not negligible. For instance, uncertainties regarding the magnitude of E derived from the ECMWF analysis for any given pentad certainly exist. For example, the mean biases between monthly averaged Comprehensive Ocean–Atmosphere Dataset (COADS) and ECMWF latent heat flux over the Indian and western Pacific Oceans are -34 and -45 W m^{-2} , respectively, most of which is due to lower ECMWF wind speeds. The correlations between monthly averaged COADS and ECMWF evaporation values over the same regions are 0.71 and 0.44, respectively (JW96). However, our contention is that the surface analyses are able to represent the slow temporal changes occurring on the timescales of the MJO. Comparing the time–space behavior of the anomalies in the surface fields (SW, E , Q , and SST) with the OLR

FIG. 4. As in Fig. 3 but for lag correlation between OLRRTS and SW anomalies. Contours and shading as in Fig. 3. Heavy (light) shaded regions indicate correlations greater (less) than 0.23 (-0.23).



anomalies tests this hypothesis. In addition, the physical and dynamical interpretations regarding the large-scale patterns of surface heat flux anomalies are drawn by comparing the results from this study with other studies that addressed the large-scale variations in the troposphere during the life cycle of the MJO (HS94).

3. Intraseasonal variability in tropical SST

Although intraseasonal variations in SST have been described in several observational studies, most of the previous studies are based on data from the Tropical Ocean Global Atmosphere Tropical Atmosphere Ocean moored buoy array in the tropical Pacific Ocean (Zhang 1996; Kessler et al. 1995). It is therefore appropriate to first examine the intraseasonal variability in the tropical SST field. We begin by investigating the power spectrum of SST in a location in the central Indian Ocean (2.5°S, 80°E). Since the focus of this study is on intraseasonal and not interannual variations, the spectrum is estimated for each year individually and then an ensemble average is computed. The following methodology is used (see also JW96): 1) the mean, linear trend, and annual cycle are removed from every year of SST time series (1985–94); 2) the resulting time series are tapered with a split-cosine bell function (5% at each end); 3) fast Fourier transform (FFT) is used to obtain raw spectral estimates for every year; 4) the raw spectral estimates are smoothed with a running average of length $L = 3$; 5) spectra computed for each year are averaged to obtain a 10-yr ensemble mean; 6) the degrees of freedom are estimated initially as 60 (2 for every raw spectral estimate $\times 3$ for smoothing the raw spectral estimates $\times 10$ for the ensemble average). The actual degrees of freedom are reduced to 56.2 due to tapering of the time series [see Madden and Julian (1971) for further details]. The red-noise background spectrum and 95% significance level are then computed following the methodology of Mitchell (1966). The SST ensemble spectrum over the central Indian Ocean is shown in Fig. 1. A broad band from 25 to 90 days exceeds the red-noise background spectrum by 95% significance level and the peak is found near 65–75 days.

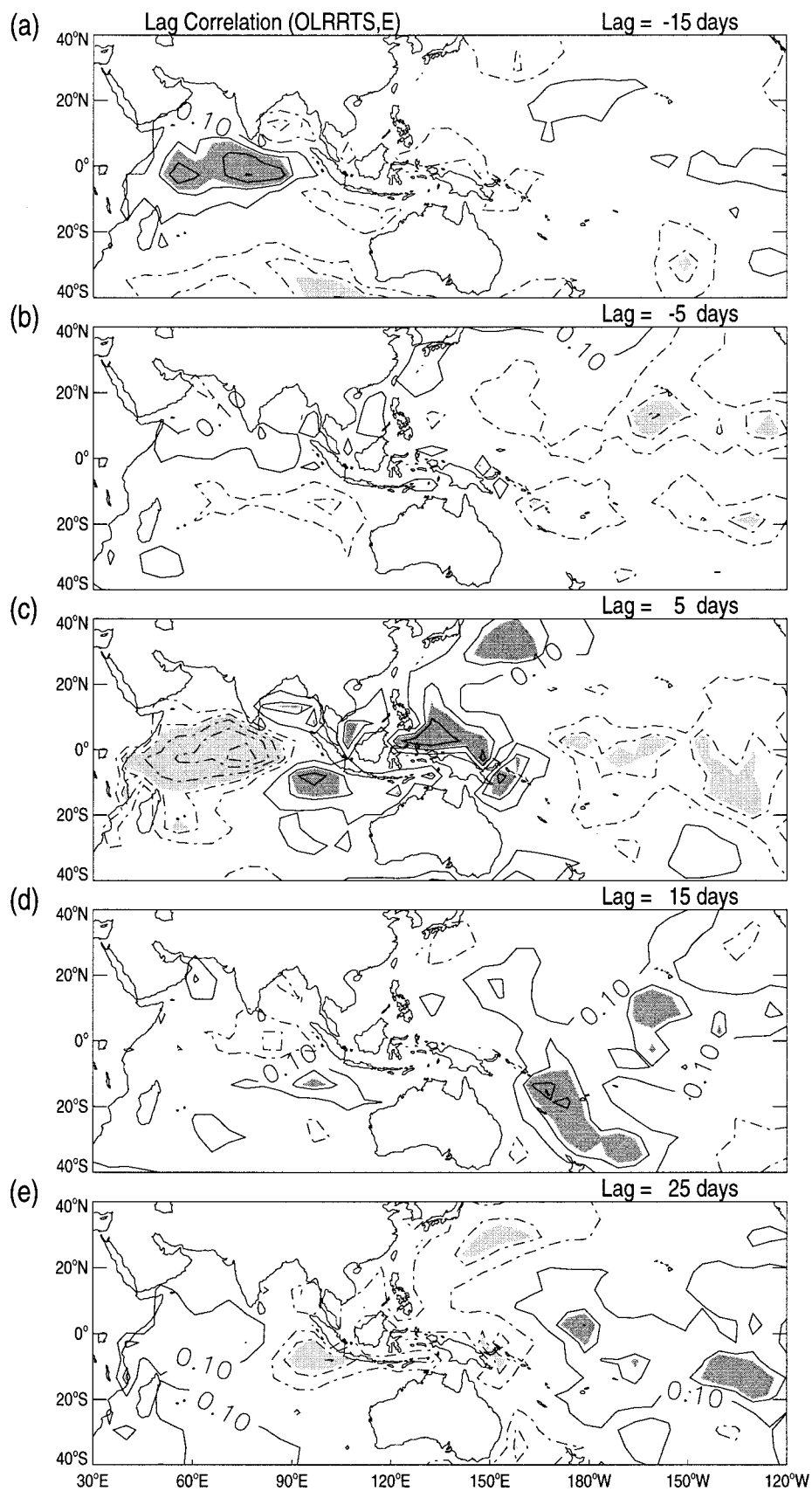
To gain further understanding into the spatial variability of the intraseasonal signal in SST, we computed the 10-yr ensemble spectrum for every grid point in the analysis domain (40°S–40°N, 0°–360°E). Next, we integrated the area under the spectrum from 25 to 90 days and divided by the total area under the spectrum. This measure gives the percentage of the intra-annual variance (excluding the annual cycle) contained in intraseasonal timescales (25–90 days) and is defined as intraseasonal variance percentage (hereafter IVP). Fur-

thermore, to emphasize only regions where the signal is present, IVP at all grid points whose spectral peaks in the 25–90 days band do not exceed the 95% significance level have been replaced with missing values. Indeed, the signal is present in virtually the entire tropical region (20°S–20°N).

The tropical IVP map (Fig. 2) shows an interesting spatial pattern with the intraseasonal oscillation in SST being detected and accounting for more than 50% of the intra-annual variance at nearly equatorial longitudes (shaded region). In the Indian Ocean the SST IVP signal is present and large over the northern region and reaches a maximum slightly south of the equator from 80°E to 90°E. Interestingly, this is the region where the MJO signal in convection is strongest (HS94). It will be shown in the next section that this region has also the highest OLR–SST correlation, which indicates strong interaction between the MJO in the convection field and the upper layers of the Indian Ocean. It is also interesting to note that the SST IVP signal reaches a minimum on the eastern coast of Africa near Tanzania and Kenya. In the Pacific Ocean, the SST IVP signal is maximum in the western (“warm pool”) and central regions and then extends to the north of the cold tongue in the eastern side of the basin. Although the intraseasonal signal in SST is also observed over the cold tongue, the amplitude is considerably less than over warm waters (IVP less than 50%). Nevertheless, ocean dynamics can play an important role in the upper-ocean energy balance in the central-eastern Pacific, for example, equatorial upwelling, and account for a large fraction of the SST intraseasonal variability in those regions. In contrast with the other basins, the SST IVP signal in the Atlantic Ocean stretches over a narrow band just north of the equator, but it is still quite strong.

What causes the tropical intraseasonal variability in SST? The SST IVP map shows that intraseasonal variability in the upper ocean has a global-scale nature being observed over all equatorial longitudes. Heating and cooling of the upper layers due to variations in the surface energy balance as well as dynamical processes in the upper ocean are the main mechanisms. Kessler et al. (1995) showed that westerly wind bursts following easterly propagating convective anomalies generate downwelling first-baroclinic-mode Kelvin waves that account for a significant part of the thermocline variability in the central and eastern Pacific Ocean. They further propose that the offset between the 40–50 days atmospheric spectral peak and the 60–75 days peak in the oceanic intraseasonal Kelvin waves arises from the relatively shorter period of the surface wind forcing and the time for the Kelvin waves to travel across wind “patches.” Likewise, another important mechanism re-

FIG. 5. As in Fig. 3 but for lag correlation between OLRRTS and E anomalies. Contours and shading as in Fig. 3. Heavy (light) shaded regions indicate correlations greater (less) than 0.23 (–0.23).



sponsible for the variability in the eastern Pacific is related to the strong meridional gradients in SST. The westward flow of cold water (South Equatorial Current) and the eastward flow of warm water (North Equatorial Countercurrent) establish large latitudinal gradients in SST over the eastern Pacific, which is known as the equatorial front (Deser et al. 1993; McPhaden 1996). Observational studies have identified westward-propagating waves along the equatorial front with wavelengths on the order of 1000 km and periods of a month (Legeckis 1977; Halpern et al. 1988; Hayes et al. 1989). In addition, numerical studies have confirmed that the instability of these waves can be largely explained by the latitudinal shear of the zonal currents (Cox 1980; Philander et al. 1986).

The mechanisms causing the intraseasonal signal in SST over longitudes other than the central and eastern Pacific where Kelvin wave activity, strong upwelling, and shear instability are not at play deserve further investigation. In the following section we focus our attention on the Indian and western Pacific Oceans and characterize the influence of the MJO on intraseasonal variations in surface heat fluxes and SST.

4. Surface heat flux variations during the MJO life cycle

To resolve low-frequency variations associated with the MJO, time filtering is first applied to the fields of OLR, SW, E , Q , and SST for the period 1–5 January 1985 through 26–30 April 1991 (total of 462 pentads). The anomalous fields are obtained by applying a band-pass Lanczos filter with frequency response of 0.5 at $0.25 \text{ pentads}^{-1}$ (20 days) and 0.05 pentad^{-1} (100 days) (see appendix for further details). A similar bandpass filter has been used by Slingo et al. (1996) in their assessment of intraseasonal oscillations in several atmospheric general circulation models.

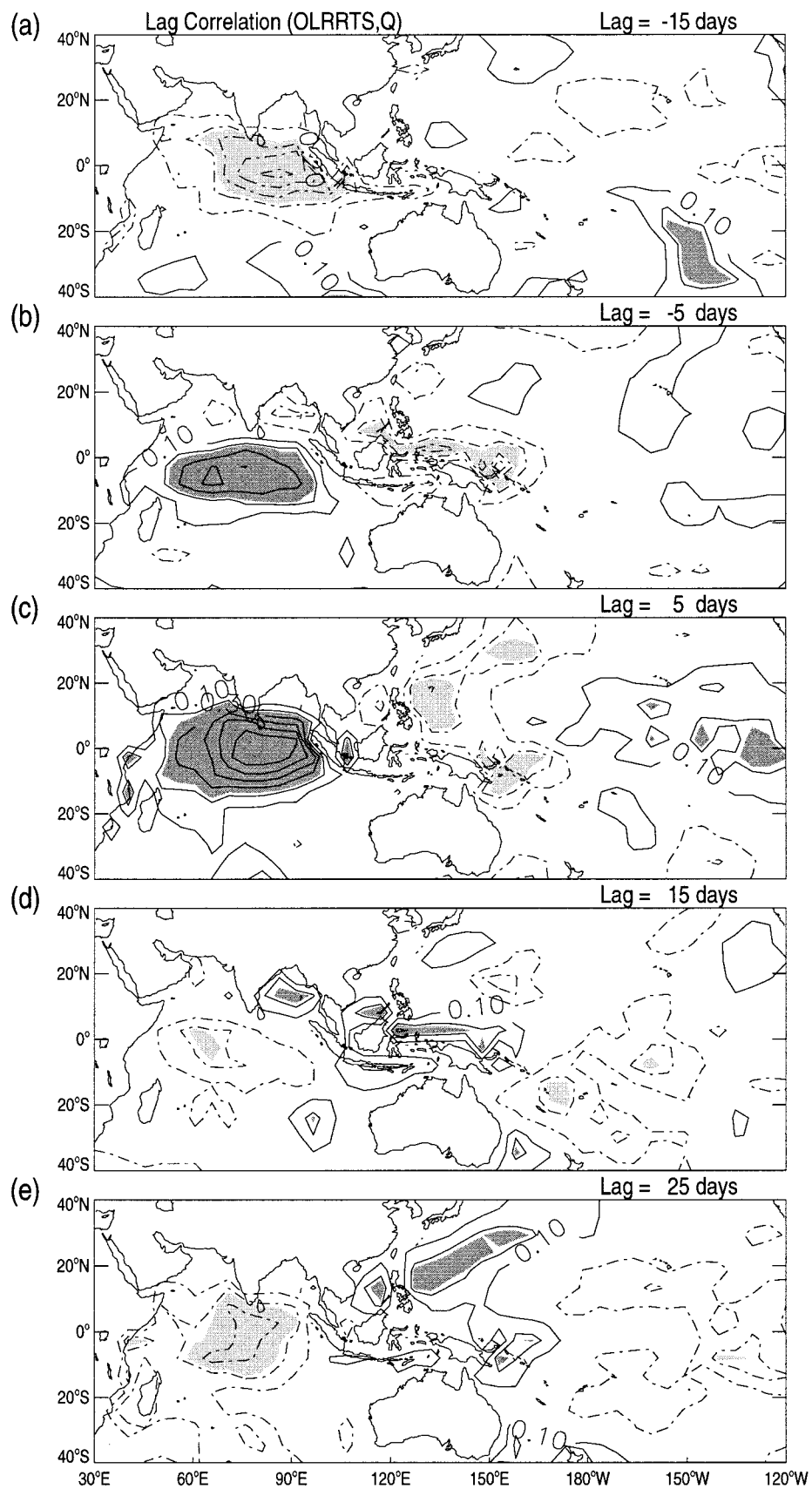
One of the most intriguing aspects of the MJO is the strong interaction between convection and the large-scale circulation as it propagates over the Indian and western Pacific Oceans (Salby and Hendon 1994). Indeed, this interaction provides the basis of virtually all present theories of the MJO (Hayashi and Golder 1993). Thus, following the practice of many previous studies (Wang and Rui 1990; HS94; JW96), we describe the processes of interest, in our case the variability of the anomalous surface heat fluxes and SST, in relation to the life cycle of convective (i.e., OLR) anomalies. We refer to positive and negative OLR anomalies as proxies for suppressed and enhanced convection, respectively. We first specify a site in the Indian Ocean (5°S – 5°N ; 80° – 90°E) from which the OLR reference time series is

taken (hereafter OLRRTS). This reference site coincides with the one used by HS94 in their composite study, and it has been noted to exhibit the largest OLR signal associated with the MJO. The spatial and temporal evolution of the MJO is investigated by computing lag correlation patterns between OLRRTS and the OLR, SW, E , Q , and SST anomalies at every grid point in the analysis domain. For convenience, we employ the same time lags used by HS94, and hence the results shown next can complement that study and provide an integrated view of the variations in convection, tropospheric large-scale circulation, surface heat fluxes, and SST during the life cycle of the MJO.

The lag correlation patterns between OLRRTS and OLR anomalies at all grid points show the time–space evolution of OLR anomalies (Fig. 3). The time lags start at -15 days and evolve up to $+25$ days at 10 days interval. Regions of positive correlations indicate that positive (negative) OLR anomalies at the reference site are correlated with positive (negative) OLR anomalies at other grid points. Following the method proposed by Livezey and Chen (1983), we determined the time between independent samples to be approximately 6 pentads. Thus, correlations larger (smaller) than $+0.23$ (-0.23) are significant at 95% level based on local t test with 69 degrees of freedom (414 pentads/6 pentads). A small region of positive correlations, initially observed on the eastern coast of Africa (lag -15 days), propagates into the central and eastern Indian Ocean (lags -5 and $+5$ days) and becomes considerably larger in spatial extent. Subsequently, the region of positive correlations propagates over Indonesia (lag $+15$ days) and splits into two small regions of positive correlations over the western Pacific Ocean (lag $+25$ days). To facilitate the discussion, we consider the situation in which the positive correlations arise from negative OLR anomalies at the reference site. In this case, the region of positive correlations can be interpreted as enhancement in convective activity associated with the MJO. Indeed, the eastward propagation of positive correlations shown in Fig. 3 is in good agreement with the composite of OLR anomalies shown in HS94, despite differences in the time period analyzed and methodology.

Figure 4 shows the lag correlation patterns between OLRRTS and the SW anomaly field. Regions of positive correlations indicate that positive (negative) OLR anomalies at the reference site are correlated with positive (negative) SW at other grid points. Readily apparent is the strong correspondence in time and space between the regions of positive and negative correlations shown in Figs. 3 and 4, respectively. If one interprets the regions of positive correlations (Fig. 4) as arising from negative OLR anomalies at the reference site and neg-

FIG. 6. As in Fig. 3 but for lag correlation between OLRRTS and Q anomalies. Contours and shading as in Fig. 3. Heavy (light) shaded regions indicate correlations greater (less) than 0.23 (-0.23).



ative SW anomalies, the correlation patterns indicate that associated with regions of enhancement in convection there is a decrease in the net surface shortwave radiation. The reverse situation is also true, that is, regions of suppressed convection are associated with an increase in net surface shortwave radiation. The fact that OLR and SW anomalies are spatially and temporally coherent is not all surprising, since the cloud field strongly affects the shortwave radiation transfer in the atmosphere (e.g., Gautier and DiJulio 1990). The important feature at play is the zonal asymmetry that the eastward propagation of the MJO induces in the net shortwave radiation flux reaching the ocean surface. The spatial pattern of SW anomalies, coupled to variations in the other components of the surface energy balance, for example, latent heat flux, likely plays an important role in the observed intraseasonal variability in SST in the Indian and western Pacific Oceans.

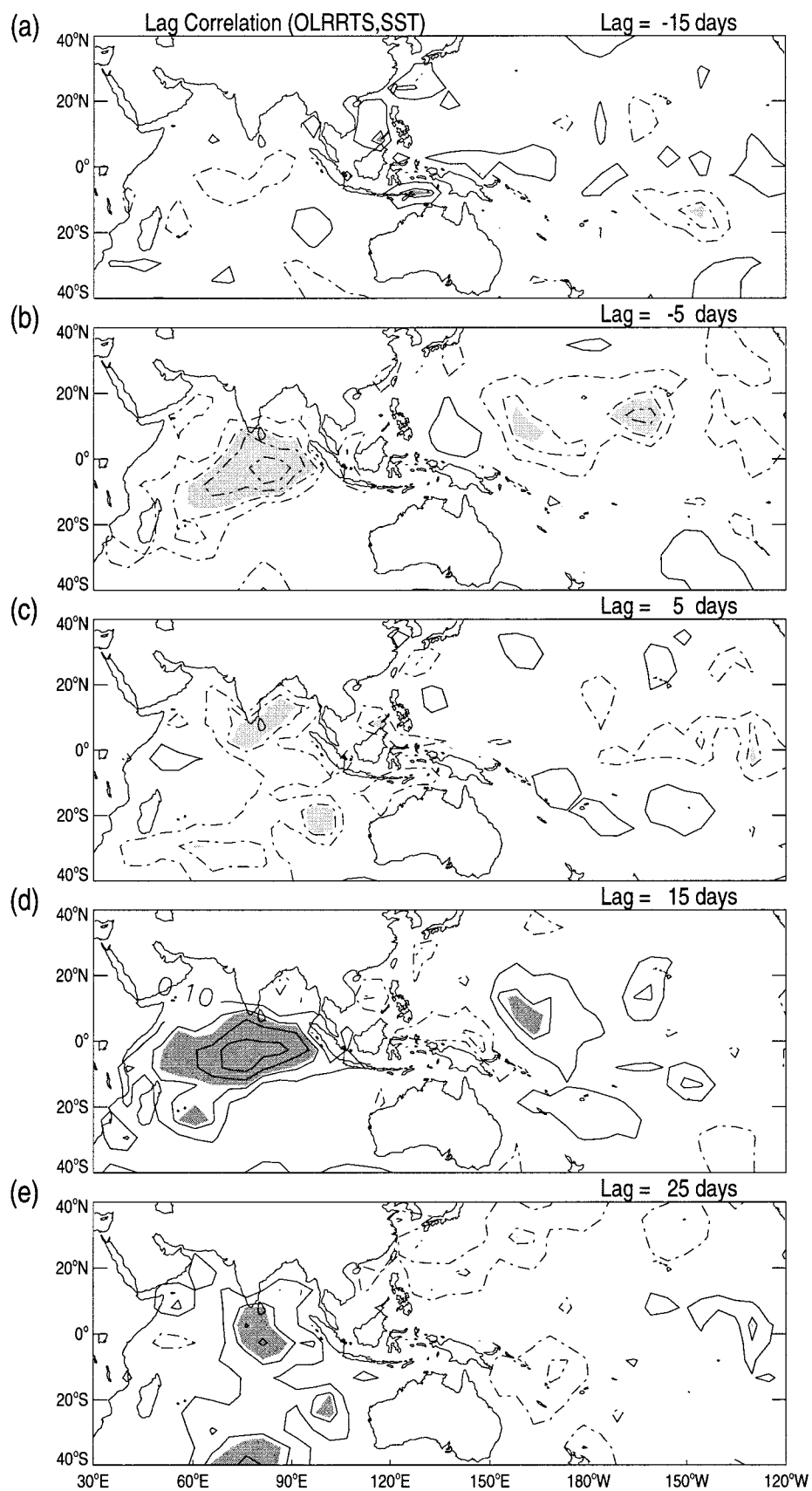
Convective activity in the MJO is also related to variations in surface latent heat flux, as can be inferred from the lag correlations between OLRRTS and E anomalies (Fig. 5). Regions of positive correlations indicate that positive (negative) OLR anomalies at the reference site are correlated with positive (negative) E anomalies. A region of positive correlations is observed in the central Indian Ocean at lag -15 days and seems to propagate toward the western Pacific at lag $+5$ days. In contrast, a large region of negative correlations forms over the Indian Ocean at lag $+5$ days. Afterward, the regions of positive correlations propagate farther east into the western Pacific Ocean (lags $+15$ and $+25$ days), whereas the region of negative correlations decreases in spatial extent and move over Indonesia ($+25$ days). A comparison of Figs. 3 and 5 suggest that negative E anomalies are observed to the east of the region of negative OLR anomalies. Likewise, positive E anomalies are located to the west of enhanced convection, as can be deduced from negative OLR anomalies. Further evidence for the eastward propagation of OLR and E anomalies is shown later in this section. Nevertheless, the spatial and temporal patterns shown in Fig. 5 are in agreement with JW96 results, which show that the decrease in E preceding the occurrence of convective anomalies is due to decreased surface wind speeds and increased surface moisture convergence. In contrast, the increase in E following the convective anomalies is related to westerly wind bursts. These features can be further inferred from the anomalous low-level circulation shown in HS94. JW96 also emphasize that the observed relationships between convective anomalies and surface latent heat fluxes contrast with the assumptions of the evaporation-wind feedback mechanism (Emanuel 1987; Neelin et al. 1987).

As discussed above, the MJO involves pronounced variations in convection and large-scale circulation that significantly modify the surface net shortwave radiation and latent heat fluxes. These variations on the other hand strongly affect the difference between SW and E , an estimate of the surface energy balance. This is shown in the lag correlation patterns between OLRRTS and Q anomalies (Fig. 6). Regions of positive correlations indicate that positive (negative) OLR anomalies at the reference site are correlated with positive (negative) Q anomalies. A comparison between Figs. 3 and 6 suggests that in the region of positive OLR anomalies, positive Q anomalies are observed. This results from positive SW anomalies and negative E anomalies. Likewise, in the region of negative OLR anomalies, negative Q anomalies are seen, and these arise from negative SW anomalies and positive E anomalies. It is also interesting to note that the evolution of Q anomalies resembles the development of SW anomalies, suggesting a predominance of anomalies in net surface shortwave radiation over surface latent heat flux anomalies.

The eastward propagation of positive Q anomalies suggests that the region of positive OLR anomalies that precede the occurrence of negative OLR anomalies favor the formation of positive SST values. This occurs because there is likely net heat gain in the upper ocean. In contrast, the eastward movement of negative OLR anomalies induces negative SST anomalies due to net oceanic heat loss. To further demonstrate this point, Fig. 7 shows the lag correlation patterns between OLRRTS and SST anomalies. Regions of positive correlations indicate that positive (negative) OLR anomalies at the reference site are correlated with positive (negative) SST anomalies. We note that a large region of negative correlations form in the Indian Ocean at lag -5 days and later decrease in spatial extent at lag $+5$ days. For easy interpretation, one can assume that the region of negative correlations arises from negative OLR anomalies at the reference site correlated with positive SST anomalies. This indicates that positive SST anomalies lead variations in negative OLR anomalies (lags -15 , -5 days). After the region of negative OLR anomalies moves toward Indonesia (cf. with Fig. 3), negative SST anomalies form over the Indian Ocean at lags $+15$ and $+25$ days). Although no statistically significant correlations are observed in the western Pacific Ocean, it is shown next that positive SST anomalies consistently lead variations of negative OLR anomalies along the equatorial region in the Indian and western Pacific Oceans.

The phase relationship between OLR and SST anomalies is further investigated by computing lag correlations between pairs of time series along the equator

FIG. 7. As in Fig. 3 but for lag correlation between OLRRTS and SST anomalies. Contours and shading as in Fig. 3. Heavy (light) shaded regions indicate correlations greater (less) than 0.23 (-0.23).



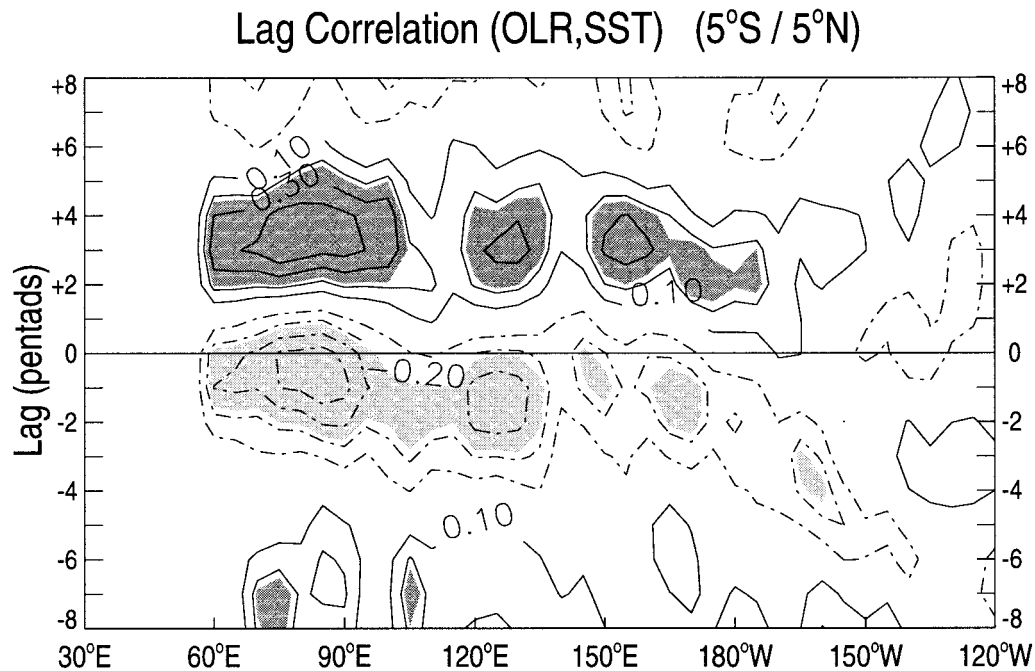


FIG. 8. Lag correlations between pairs of OLR and SST anomalies along the equator and averaged from 5°S to 5°N. Negative lags indicate that SST leads variations in OLR anomalies. Heavy (light) shaded regions indicate correlations greater (less) than 0.23 (−0.23) and are significant at 95% significance level based on local t test.

averaged from 5°S to 5°N for every longitude in the Indian and Pacific Oceans. The statistical significance is based on a local t test based on 69 degrees of freedom. Figure 8 shows lag correlations between OLR and SST anomalies such that negative lag correlations imply that positive SST anomalies lead variations of negative OLR anomalies. The negative correlations at −1 and −2 pentads further indicate that positive SST anomalies lead variations in negative OLR anomalies along the entire equatorial domain. However, it is interesting to note that correlations are higher in the Indian Ocean than in the western Pacific. In addition, in the Indian Ocean, SST leads OLR by one pentad, while SST leads OLR by two and three pentads in the western and central Pacific, respectively, which is consistent with other studies of the MJO (Kawamura 1988; Zhang 1996).

The propagation of convective anomalies associated with MJO events in the Indian and Pacific Ocean is known to exhibit a complex behavior, sometimes appearing as a quasi-standing oscillation and other times as an eastward-moving disturbance (Wang and Rui 1990; Madden and Julian 1994; Zhang and Hendon 1997). The lag correlation patterns (Figs. 3–7) and OLR–SST time series correlations along the equator (Fig. 8) shown above are based on nearly 6 yr of data. In addition to including different types of MJO events, the time series also contain variations not necessarily related to the oscillation itself (e.g., noise in the time series). To further illustrate the relationships between OLR, SW, E , Q , and SST anomalies using a different statistical technique,

the following figures show composites of OLR, SW, E , Q , and SST anomalies. The time versus longitude composites were performed by averaging the anomalies in latitude between 5°N and 5°S. The events to compute the composites were selected when the OLR anomaly in the western Pacific (150°E) was less than -27 W m^{-2} and therefore emphasize strong MJO occurrences. A total of 22 OLR events during 1985–94 were selected and used to compute the composites of OLR, E , and SST. The SW and Q composites are based on the first 18 events only given the shorter record of ISCCP data.

Figure 9 shows the time-longitude composite of OLR anomalies. Clearly seen is the eastward propagation of negative (shaded) OLR anomalies originating in the Indian Ocean and propagating into the western Pacific (vertical line). At lag 0 days, the composite of OLR anomalies in the western Pacific is as low as -30 W m^{-2} . As discussed before the cloud field strongly modifies the transfer of shortwave radiation in the atmosphere. Figure 10 shows the SW composite and further demonstrates the influence of the MJO in introducing negative (unshaded) and positive (shaded) anomalies in the surface shortwave radiation. The region of negative anomalies in SW (unshaded) nearly overlays the region of negative OLR anomalies. In the western Pacific at lag 0 days, the composite of SW anomalies is as low as -20 W m^{-2} . The eastward movement of E anomalies (Fig. 11) follows the propagation of negative OLR anomaly. Furthermore, the positive E anomalies (shaded) lag the variations of negative OLR anomalies by

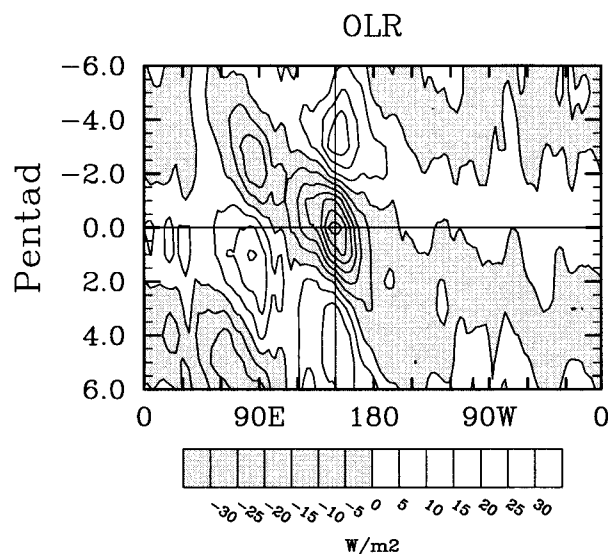


FIG. 9. Time-longitude composite of OLR anomalies during 1985–94. The composite was computed by selecting events in which the OLR anomaly at 150°E (indicated by the vertical line) was less than -27 W m^{-2} . There were a total of 22 events. Shaded regions indicate negative OLR anomalies.

about 1–2 pentads. At lag +2 pentads in the western Pacific, the composite of positive E anomalies is as high as 12 W m^{-2} . Figure 12 shows the eastward movement of anomalies in Q . It is interesting to note that OLR and Q are slightly out of phase at lag 0 days, which arises from the in-phase and out-of-phase relationships between OLR–SW and OLR– E , respectively. In addition, at lag +1 day in the western Pacific, the composite of negative (unshaded) SW anomalies can be as low as

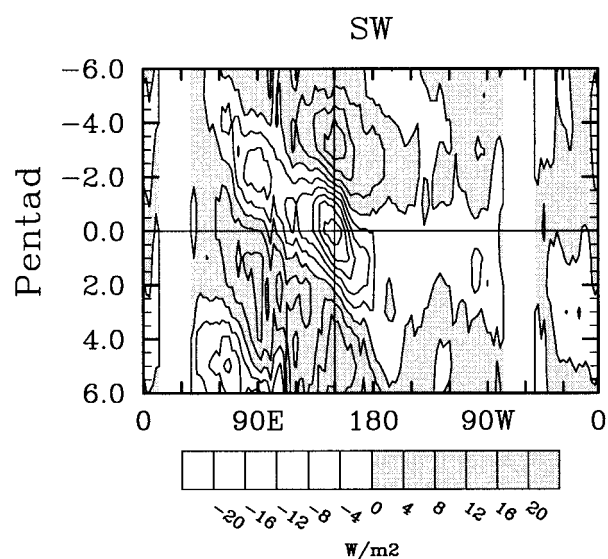


FIG. 10. Similar to Fig. 9 but for SW anomalies. Composite is based on the first 18 events used in the OLR composite. Shaded regions indicate positive SW anomalies.

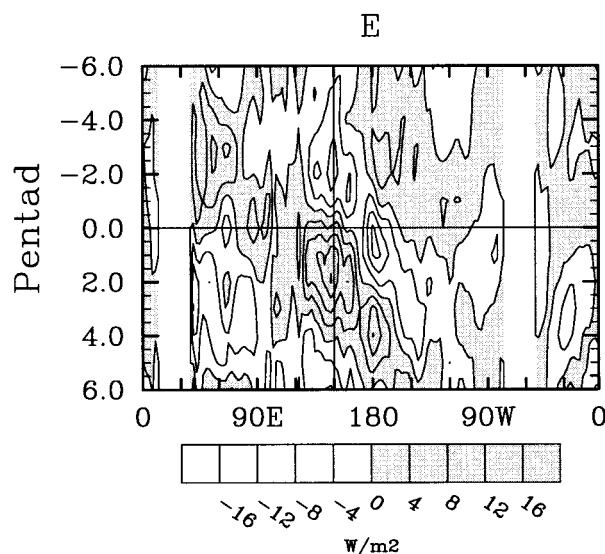


FIG. 11. Similar to Fig. 9 but for E anomalies. Composite is based on the same 22 events used in the OLR composite. Shaded regions indicate positive E anomalies.

-30 W m^{-2} . Associated with eastward propagation of OLR, SW, E , and Q anomalies, Fig. 13 suggests eastward propagation of SST anomalies. As discussed before, positive anomalies of SST (shaded region) lead variations of negative OLR anomalies by 1–3 pentads.

5. Summary and discussion

This paper examined the association between the MJO and intraseasonal variations in surface heat fluxes

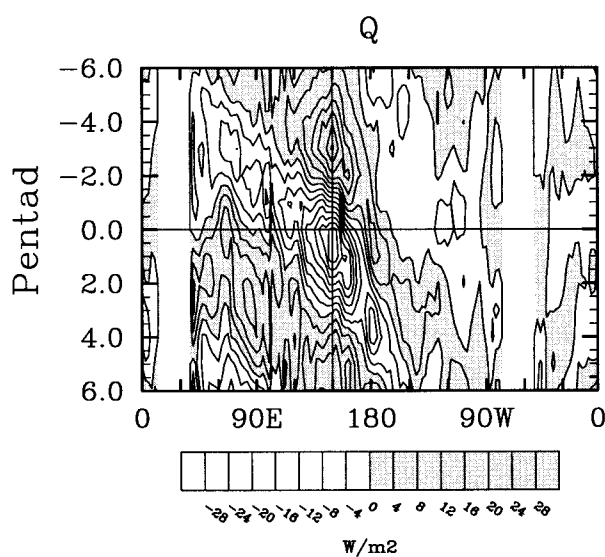


FIG. 12. Similar to Fig. 9 but for Q anomalies. Composite is based on the first 18 events used in the OLR composite. Shaded regions indicate positive Q anomalies.

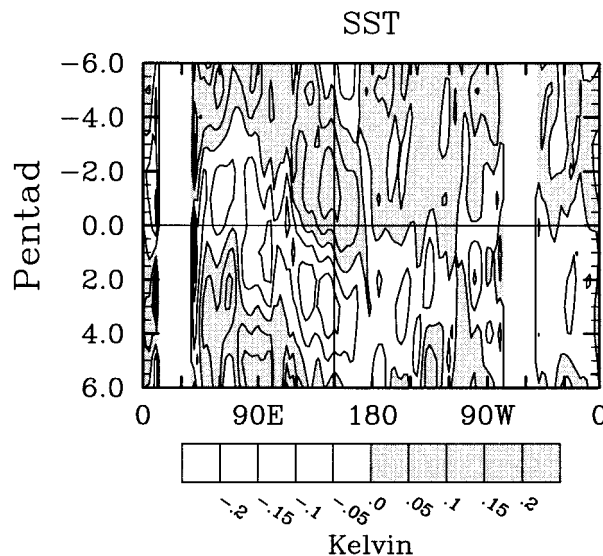


FIG. 13. Similar to Fig. 9 but for SST anomalies. Composite is based on the same 22 events used in the OLR composite. Shaded regions indicate positive SST anomalies.

and SST in the Indian and Pacific Oceans. A spectral analysis of SST shows additional observational evidence that intraseasonal variations in SST occur in each of the tropical oceans, over a wide latitudinal domain. Although the MJO reaches maximum amplitudes over the Indian and western Pacific Oceans, intraseasonal spectral peaks in SST are detected along the entire tropical region including the Atlantic Ocean. This raises the important questions of what are the driving mechanisms of the oscillation in SST and how the SST intraseasonal variability may feedback onto the oscillation. This study focused on the Indian and western Pacific Oceans, and it was shown that the variations in convection and large-scale atmospheric circulation strongly modify the ocean surface fluxes of net shortwave radiation and latent heat. Variations in these components of the surface energy balance influence the variations in SST. Dynamical mechanisms, not examined in this study, are likely responsible for variations in SST in regions of strong horizontal gradients such as the central and eastern Pacific Ocean.

Based on previous studies along with results presented here, an integrated view of the MJO can be summarized in this way. In the lower and upper troposphere of the Eastern Hemisphere, the intense interaction between convection and large-scale circulation originates an eastward propagating response that resembles a coupled Rossby–Kelvin wave pattern. In contrast, near the dateline where the interaction between convection and large-scale circulation decreases, the response appears as radiant Kelvin waves (HS94). As the associated system of suppressed and enhanced convection propagates across the Indian and western Pacific Oceans, large fluctuations take place near the

surface. Before the occurrence of convective anomalies, clear skies are observed near the surface. In addition, surface wind speeds are minimum before the occurrence of convection and low-level moisture convergence is maximum (HS94; JW96). These prevailing conditions induce increased surface net shortwave radiation and decreased surface latent heat fluxes, implying positive anomalies in the difference $Q = SW - E$. These conditions favor positive anomalies of SST. On the other hand, the positive anomalies of SST lead variations in convection. As the convective anomalies propagate eastward across the region, the increase in cloudiness and surface wind speeds due to westerly wind bursts causes a decrease in the net surface shortwave radiation and increase in surface latent heat fluxes, which result in negative Q anomalies conditions and favor negative SST anomalies.

Although changes in the surface net shortwave radiation and latent heat fluxes during the life cycle of the MJO significantly contribute to the SST variability, they are not the only processes that determine the oscillation in SST. The relevance of the other two terms of the surface energy balance, net longwave radiation and sensible heat fluxes, as well as the dynamics of the upper-equatorial ocean are also important. It is quite possible that the mechanisms that drive the SST oscillation vary with geographical location. As shown by Kessler et al. (1995), forced intraseasonal Kelvin waves have a fundamental role in the thermocline variability of the central and eastern Pacific Ocean where horizontal gradients in SST and upwelling are significant. Likewise, latitudinal shear in SST along the equatorial front excites westward-propagating waves that account for a significant part of the variability in SST in the eastern Pacific (McPhaden 1996). In the Indian and western Pacific Oceans, variations in convection and consequently in net surface shortwave radiation are dramatic, whereas in the equatorial Atlantic they are less pronounced. In contrast, surface latent heat fluxes exhibit sharp intraseasonal spectral peaks in all oceans (JW96), which are indicative of the importance of anomalies in the low-level circulation in modifying the surface energy balance.

Present theories suggest that the MJO is generated by dynamical mechanisms internal to the atmosphere (Hayashi and Golder 1993; Salby et al. 1994; Hendon and Salby 1996). However, the oscillation is also coupled to air–sea interaction processes such as variations in surface heat fluxes and SST. The results presented here provide further evidence of an important relationship between the variability in the MJO, surface heat fluxes (SW and E), and SST that is at odds with some of the present theories (e.g., evaporation–wind feedback). This relationship strongly suggests that an examination of the coupled behavior between the MJO and SST (Kawamura 1988) be undertaken and the authors are presently pursuing this latter topic.

Acknowledgments. The authors would like to specially thank Dr. Tim Liu for providing his computer code to estimate surface latent heat fluxes and continuing support, and Dr. Paul Ricchiazzi, James Marquez, and Pete Peterson for help with data processing and graphics. The authors also greatly acknowledge data support provided by the National Center for Atmospheric Research, which is sponsored by the National Science Foundation. This work is supported by National Science Foundation research Grants ATM9319483 (CJ and CG) and ATM-9420833 (DEW) as well as by the National Aeronautics and Space Administration Grant NASA-JPL959177 (CJ and CG).

APPENDIX

Time Filtering

To describe intraseasonal variations associated with the MJO, a Lanczos bandpass filter is used with 49 weights defined as:

$$w_k = [\sin(2\pi f_{c_2} k)/\pi k - \sin(2\pi f_{c_1} k)/\pi k]\sigma,$$

where $\sigma = [\sin(\pi k/n)]/(\pi k/n)$; $k = -n, \dots, 0, \dots, n$; and $n = 24$. The cut-in and cut-out frequencies f_{c_1} and f_{c_2} , respectively, are equal to $0.25 \text{ pentads}^{-1}$ (20 days) and 0.05 pentad^{-1} (100 days). Figure A1 shows the frequency response of this bandpass filter, which indicates minimum Gibbs oscillation near f_{c_1} and f_{c_2} . Additional details on Lanczos filter are described in Duchon (1979).

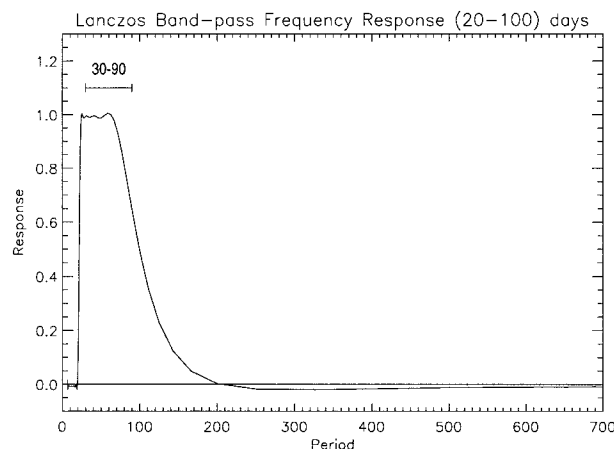


FIG. A1. Frequency response of Lanczos bandpass filter. The band (30–90) days is indicated at the top and has frequency response approximately equal to 1.

REFERENCES

- Chelliah, M., and P. Arkin, 1992: Large-scale interannual variability of monthly outgoing longwave radiation anomalies over the global Tropics. *J. Climate*, **5**, 371–389.
- Chen, T.-C., and J. C. Alpert, 1990: Systematic errors in the annual and intraseasonal variations of the planetary-scale divergent circulation in NMC medium-range forecasts. *Mon. Wea. Rev.*, **118**, 2607–2623.
- Cox, M. D., 1980: Generation and propagation of 30-day waves in a numerical model of the Pacific. *J. Phys. Oceanogr.*, **10**, 1168–1186.
- Deser, C., J. J. Bates, and S. Wahl, 1993: The influence of sea surface temperature gradients on stratiform cloudiness along the equatorial front in the Pacific Ocean. *J. Climate*, **6**, 1172–1180.
- Duchon, C. E., 1979: Lanczos filter in one and two dimensions. *J. Appl. Meteor.*, **18**, 1016–1022.
- ECMWF, 1992: Research Manual 1: ECMWF data assimilation scientific documentation. European Centre for Medium-Range Weather Forecasts, Meteorological Bulletin M1.5/1, 83 pp. [Available from ECMWF, Reading RG2 9AX, United Kingdom.]
- Emanuel, K. A., 1987: An air–sea interaction model of intraseasonal oscillations in the tropics. *J. Atmos. Sci.*, **44**, 2324–2340.
- Enfield, D. B., 1987: The intraseasonal oscillation in eastern Pacific sea levels: How is it forced? *J. Phys. Oceanogr.*, **17**, 1860–1876.
- Fairall, C. W., E. F. Bradley, J. S. Godfrey, G. A. Wick, J. B. Edson, and G. S. Young, 1996: Cool-skin and warm-layer effects on sea surface temperature. *J. Geophys. Res.*, **101**, 1295–1308.
- Ferranti, L., T. N. Palmer, F. Monteni, and E. Klinker, 1990: Tropical–extratropical interaction associated with the 30–60-day oscillation and its impact on medium and extended range prediction. *J. Atmos. Sci.*, **47**, 2177–2199.
- Gautier, C., and B. DiJulio, 1990: Cloud effects on air–sea interactions during 1979 Indian summer monsoon as studied from satellite observations. *Meteor. Atmos. Phys.*, **44**, 251–263.
- , and M. Landsfeld, 1997: Surface solar radiation flux and cloud radiative forcing for the atmospheric radiation measurement (ARM) southern Great Plains (SGP): A satellite, surface observations and radiative transfer model study. *J. Atmos. Sci.*, **54**, 1289–1307.
- , G. Diak, and S. Masse, 1980: A simple physical model to estimate incident solar radiation at the surface from GOES satellite data. *J. Appl. Meteor.*, **19**, 1005–1012.
- Halpern, D. R., A. Knox, and D. S. Luther, 1988: Observations of 20-day period meridional current oscillations in the upper ocean along the Pacific equator. *J. Phys. Oceanogr.*, **18**, 1514–1534.
- Hayashi, Y., and D. G. Golder, 1993: Tropical 40–50 and 25–30 day oscillations appearing in realistic and idealized GFDL climate models and ECMWF data set. *J. Atmos. Sci.*, **50**, 464–494.
- Hayes, S. P., M. J. McPhaden, and J. M. Wallace, 1989: The influence of sea surface temperature on surface wind in the eastern equatorial Pacific: Weekly to monthly variability. *J. Climate*, **2**, 1500–1506.
- Hendon, H. H., and M. L. Salby, 1994: The life cycle of the Madden and Julian oscillation. *J. Atmos. Sci.*, **51**, 2225–2237.
- , and —, 1996: Planetary-scale circulations forced by intraseasonal variations of observed convection. *J. Atmos. Sci.*, **53**, 1751–1758.
- Jones, C., and B. C. Weare, 1996: The role of low-level moisture convergence and ocean latent heat fluxes in the Madden and Julian oscillation: An observational analysis using ISCCP data and ECMWF analyses. *J. Climate*, **9**, 3086–3104.
- Kawamura, R., 1988: Intraseasonal variability of sea surface temperatures over the tropical western Pacific. *J. Meteor. Soc. Japan*, **66**, 1007–1012.
- Kessler, W. S., M. J. McPhaden, and K. M. Weickmann, 1995: Forcing of intraseasonal Kelvin waves in the equatorial Pacific. *J. Geophys. Res.*, **100**, 10 613–10 631.
- Krishnamurti, T. N., D. K. Oosterhof, and A. V. Mehta, 1988: Air–sea interaction on the time scale of 30 to 50 days. *J. Atmos. Sci.*, **45**, 1304–1322.
- Lau, K. M., and P. H. Chan, 1986a: Aspects of the 40–50 day oscillation during the northern summer as inferred from outgoing longwave radiation. *Mon. Wea. Rev.*, **114**, 1354–1367.
- , and —, 1986b: The 40–50 day oscillation and the El Niño/

- Southern Oscillation: A new perspective. *Bull. Amer. Meteor. Soc.*, **67**, 533–534.
- , and F. C. Chang, 1992: Tropical intraseasonal oscillation and its prediction by the NMC operational model. *J. Climate*, **5**, 1365–1378.
- Legeckis, R., 1977: Long waves in the eastern equatorial Pacific Ocean: A view from a geostationary satellite. *Science*, **197**, 1179–1181.
- Li, T., and B. Wang, 1994: The influence of sea surface temperature on the tropical intraseasonal oscillation: A numerical study. *Mon. Wea. Rev.*, **122**, 2349–2362.
- Liu, W. T., K. B. Katsaros, and J. A. Businger, 1979: Bulk parameterization of air–sea exchanges of heat and water vapor including molecular constraints at the surface. *J. Atmos. Sci.*, **36**, 1722–1735.
- Livezey, R. E., and W. Y. Chen, 1983: Statistical field significance and its determination by Monte Carlo techniques. *Mon. Wea. Rev.*, **111**, 46–59.
- Madden, R. A., and P. R. Julian, 1971: Detection of a 40–50 day oscillation in the zonal wind in the tropical Pacific. *J. Atmos. Sci.*, **28**, 702–708.
- , and —, 1994: Observations of the 40–50-day tropical oscillation: A review. *Mon. Wea. Rev.*, **122**, 814–837.
- McPhaden, M. J., 1996: Monthly period oscillations in the Pacific North Equatorial Countercurrent. *J. Geophys. Res.*, **101**, 6337–6359.
- , and S. P. Hayes, 1991: On the variability of winds, sea surface temperature, and surface layer heat content in the western equatorial Pacific. *J. Geophys. Res.*, **96**, 3331–3342.
- Mitchell, J. M., Jr., 1966: Climate change. World Meteorological Organization Tech. Note 79, 79 pp. [Available from WMO, 41 Avenue Giuseppe-Motta-1211, Geneva 2, Switzerland.]
- Neelin, J. D., I. M. Held, and K. H. Cook, 1987: Evaporation–wind feedback and low-frequency variability in the tropical atmosphere. *J. Atmos. Sci.*, **44**, 2341–2348.
- Philander, S. G. H., W. J. Hurlin, and R. C. Pacanowski, 1986: Properties of long equatorial waves in models of the seasonal cycle in the tropical Atlantic and Pacific Oceans. *J. Geophys. Res.*, **91**, 14 207–14 211.
- Reynolds, R. W., and T. M. Smith, 1994: Improved global sea surface temperature analyses using optimal interpolation. *J. Climate*, **7**, 929–948.
- Rossow, W. B., L. C. Garder, P. J. Lu, and A. W. Walker, 1988: International Satellite Cloud Climatology Project (ISCCP) documentation of cloud data. World Meteorological Organization WMO/TD 266, 78 pp. [Available from WMO, 41 Avenue Giuseppe-Motta-1211, Geneva 2, Switzerland.]
- Salby, M. L., and H. H. Hendon, 1994: Intraseasonal behavior of clouds, temperature and motion in the Tropics. *J. Atmos. Sci.*, **51**, 2207–2224.
- , R. Garcia, and H. H. Hendon, 1994: Planetary circulations in the presence of climatological and wave-induced heating. *J. Atmos. Sci.*, **51**, 2344–2367.
- Slingo, J. M., and Coauthors, 1996: Intraseasonal oscillations in 15 atmospheric general circulation models: Results from an AMIP diagnostic subproject. *Climate Dyn.*, **12**, 325–357.
- Waliser, D. E., 1996: Formation and limiting mechanisms for very high sea surface temperature: Linking the dynamics and thermodynamics. *J. Climate*, **9**, 161–188.
- , and W. Zhou, 1997: Removing satellite equatorial crossing time biases from the OLR and HRC datasets. *J. Climate*, **10**, 2125–2146.
- , N. E. Graham, and C. Gautier, 1993: Comparison of the highly reflective cloud and outgoing longwave datasets for use in estimating tropical deep convection. *J. Climate*, **6**, 331–353.
- Wang, B., and H. Rui, 1990: Synoptic climatology of transient tropical intraseasonal convection anomalies: 1975–1985. *Meteor. Atmos. Phys.*, **44**, 43–61.
- Weickmann, K. M., 1991: El Niño/Southern Oscillation and Madden-Julian (30–60 day) oscillations during 1981–1982. *J. Geophys. Res.*, **96**, 3187–3195.
- Zhang, C., 1996: Atmospheric intraseasonal variability at the surface in the tropical western Pacific Ocean. *J. Atmos. Sci.*, **53**, 739–758.
- , and H. H. Hendon, 1997: On propagating and standing components of the intraseasonal oscillation in tropical convection. *J. Atmos. Sci.*, **54**, 741–752.
- Zhang, G. J., and M. J. McPhaden, 1995: On the relationships between sea surface temperature and latent heat flux in the equatorial Pacific. *J. Climate*, **8**, 589–605.